Journal of Materials Processing Technology, Volume 288, February 2021, Article number 116842
DOI: 10.1016/j.jmatprotec.2020.116842

The effect of wire size on high deposition rate wire and plasma arc additive manufacture of Ti-6Al-4V

Chong Wang*, Wojciech Suder, Jialuo Ding, Stewart Williams

Welding Engineering and Laser Processing Centre, Cranfield University, Cranfield MK43 0AL, UK

***Corresponding author:** chong.wang1@cranfield.ac.uk

Abstract

Wire + arc additive manufacture (WAAM) is suitable for building large-scale components with high deposition rate. However, in order to further increase the deposition rate of Ti-6Al-4V to improve productivity and reduce manufacture costs without significantly compromising the quality, some fundamental process characteristics need to be investigated. In this paper, the effect of wire size on the limitation of deposition rate and bead shape in plasma arc additive manufacture was studied along with the process tolerance and melting characteristics, such as the effect of current and nozzle size on keyhole behaviour and the effect of wire feeding position on deposition process. The results show that with the same heat input the deposition rate increases linearly with the wire size due to the increasing melting efficiency. The bead geometry obtained with a thinner wire has a higher aspect ratio, which can be attributed to the difference in the distribution of the energy between wire and workpiece. The likelihood of keyhole increases with increasing current and decreasing nozzle size, and it can be mitigated by using thicker wires. The wire feeding position plays a significant role in determining the metal transfer mode, which has a great impact on the bead shape and process stability. Also, as the deposition rate changes thin wire is more sensitive to wire feeding position than thick wire in terms of metal transfer behaviour.

Keywords: Wire + arc additive manufacture; plasma transferred arc; titanium; high deposition rate; keyhole

1. Introduction

Additive manufacture (AM) is a promising technology that can be used to manufacture components by layer-upon-layer deposition of materials (Frazier, 2014). Compared to traditional subtractive manufacture, AM has distinctive advantages in the reduction of material wastage and machining effort required (DebRoy et al., 2018). Furthermore, it offers a relatively short lead time, high design freedom and low overall part costs. Numerous AM techniques have been developed to produce metallic structures, which can be classified based upon feedstock and heat source. Depending on the feedstock, AM techniques can be classified into powder based and wire based processes. In general, the powder based processes offer higher resolution and fidelity, whilst the wire based processes allow higher deposition rates. The layer thickness in a powder based process can be up to 200 μm as revealed by Shi et al. (2016), while a typical layer thickness in a wire based process is 1-2 mm as stated by Williams et al. (2016). This means that the wire based processes are more suitable for manufacturing of large-scale components where high volumes of deposited material are required. In addition, depending on the heat source, AM techniques can be split into laser based, electron beam based, and electric arc based processes. Amongst these, the arc based processes are the most versatile and cost effective, as unlike electron beam they do not require a vacuum chamber, and are more efficient than lasers. The electric arc fusion processes have been designed to efficiently melt the feedstock of wire and are widely used for welding and AM processes. They can be operated either in a global enclosure or, as demonstrated by Ding et al. (2015), out-of-chamber using a local shielding device. Hence, wire + arc additive manufacture (WAAM) offers potentially an unlimited working envelope and high deposition rate, which is optimum for the fabrication of large-scale and medium-complex components.

In WAAM, various arc processes can be employed to serve as energy source, including gas metal arc (GMA), gas tungsten arc (GTA), and plasma transferred arc (PTA). GMA with coaxially incorporated filler wire is commonly used in deposition of steel and aluminium alloys, but as shown by Pardal et al. (2019) it suffers from a significant arc wandering, spatter and poor surface quality in alloys with low work function, including titanium. GTA and PTA with non-consumable electrodes do not suffer from this issue and allow high quality deposition with a wide range of materials. Compared to GTA, PTA has a higher stand-off distance and lower risk of tungsten contamination, thereby giving a higher process tolerance. Martina et al. (2012) first used PTA to deposit titanium and developed a working envelope for the process. They concluded

that PTA based WAAM process gives higher deposition rate and larger effective wall width than other WAAM processes.

Depending on different deposition strategies, the deposition rate of titanium in WAAM processes ranges from 0.4 to 1.2 kg/h. A higher deposition rate would be desirable in order to reduce production times and therefore the overall costs, but the limit of productivity is dictated by the process physics and ability to control the melt pool shape. Williams et al. (2016) stated that high deposition rates but with poor process control leads to an excessive amount of material needing to be deposited and subsequently machined away, which is counterproductive from the economic point of view. Therefore, it is of critical significance to increase the deposition rate without compromising the quality and fidelity of the components.

Another factor limiting the deposition rate in PTA based WAAM process is arc pressure. High current induces the arc pressure upon the melt pool due to the electromagnetic force, and above a certain current level a keyhole is generated, as shown by Wang et al. (2017). In welding, the keyhole is beneficial as a means of improving penetration depth and productivity. In AM, however, the keyhole is undesirable as it leads to defects formation and poor efficiency. High penetration depth means unnecessarily remelting of the underlying layers, which consequently reduces the process efficiency and may increase distortion in the components. Therefore it is important to understand the process limit and melting behaviour in order to maximise the feedstock melting and minimise penetration into the underlying layers.

Efficient feedstock melting is another important aspect in high deposition rate WAAM. One of the effective ways of improving deposition rate is to increase the wire feed speed (WFS) whilst increasing the energy input by using a higher current. For a given energy input, in order to feed the material more quickly, there are different combinations of the wire size and WFS. For example, we can use either a thin wire with a high WFS or a thick wire with a low WFS. However, it needs to be understood which combination is more efficient. Moreover, with the same deposition rate and energy input, the bead shape and its quality is dependent on the melting behaviour of the wire. Ríos et al. (2019) studied the metal transfer behaviour in PTA based WAAM process by analysing the voltage waveform and video imaging, and stated that depending on the position of the feedstock in the arc, different metal transfer modes can be achieved, which affects the process stability and even bead quality. Chu and Lian (2004) reported that the arc source does not have a uniform energy distribution and therefore there is a steep temperature gradient across the plasma arc, which means different regions of the arc have different temperature distributions. Therefore, the process is sensitive

to the wire position with respect to the arc column. Also, the wire diameter should play an important role in melting efficiency of wire and metal transfer mode, which is a key factor in improving deposition rate of WAAM. However, all the effects of wire size on process characteristics and deposition rate in PTA based WAAM are not well understood.

In this work, the effect of wire diameter and feeding rate on the deposition rate and melting characteristics in PTA based WAAM of Ti-6Al-4V was studied. The main focus was to investigate which combination of wire diameter and WFS can give higher deposition rate and better bead geometry and how to control the process and avoid defects at high deposition rate WAAM. All aspects of limitation of deposition rate, bead shape control, keyhole formation and metal transfer were studied.

2. Experimental procedure

2.1 Materials and setup

Deposition was performed on Ti-6Al-4V substrates with dimensions of 300 mm × 200 mm × 7 mm. Four different sized Ti-6Al-4V wires with 1.2, 1.6, 2.0 and 2.4 mm diameters were used as feedstock. The chemical compositions of the substrates and wires are listed in Table 1. The shielding gas and the plasma gas were pure argon (99.99 %). Fig. 1 shows a schematic diagram of the experimental setup. The substrate was fixed onto an aluminium baseplate by means of M8 bolts, and the baseplate was clamped on the workbench. Before deposition, the substrates were polished and then cleaned with acetone to remove any surface contamination. For the WAAM system, a DC plasma power supply (EWM Tetrix 352) was used and an arc monitor (AMV 4000) was used to record the arc voltage and current. The motion of the torch was provided by a computer numerical controlled (CNC) gantry system. A Lincoln wire feeder was used to feed the wire, and a CMOS process camera (Xiris XVC-1000) was used to record the melt pool and the wire melting behaviour. The camera recording rate and resolution were 55 fps and 1280×1024 respectively. The experiments were conducted in an argon-filled chamber to prevent the material from oxidation, where the chamber was purged until the oxygen level was below 500 ppm as verified by an oxygen analyser. This oxygen level was found to be optimum based on previous study by Caballero et al. (2019). Also, front feeding configuration was used. During the experiments, some process parameters were kept constant, as listed in Table 2.

Table 1 Chemical composition (in wt.%) of the Ti-6Al-4V substrate and wire.

	Al	V	Fe	C	N	H	O	Ti
Substrate	6.39	4.20	0.17	0.01	0.01	0.006	0.16	Balance
Wire	6.08	3.80	0.122	0.019	0.008	0.001	0.15	Balance

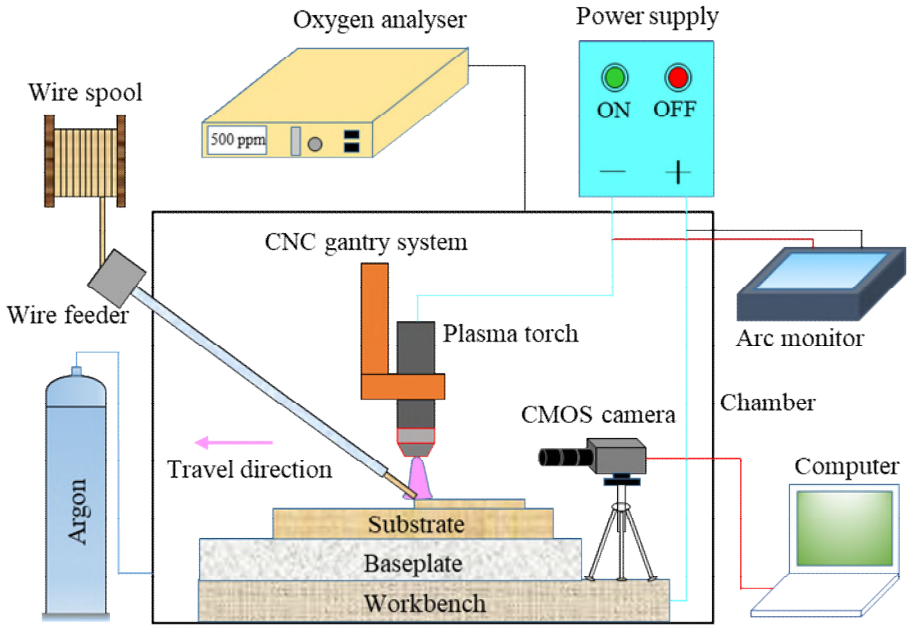

Fig. 1. Schematic diagram of the experimental setup.

Table 2 Fixed process parameters used during the experiments.

Parameters	Value (unit)
Torch travel speed	4.5 mm/s
Bead length	120 mm
Plasma gas flowrate	0.8 L/min
Shielding gas flowrate	8 L/min
Wire feeding angle	25°
Nozzle to substrate stand-off	8 mm

2.2 Methods

Four different sized wires with diameters of 1.2, 1.6, 2.0 and 2.4 mm were used to identify the optimum combination of wire diameter and WFS for high deposition rate. For each size of wire, the current was increased from 200 to 300 A with an increment of 50 A to study the effect of current on deposition rate. At each current level, the WFS was increased until a limit value of melting and stabbing which was determined from the process camera.

The effect of wire size on bead shape was studied using 1.2 and 2.4 mm wires at a constant current of 250 A. The WFSs for both wires were increased from low to high values and the range of the deposition

rates for both wires were same. After deposition, the samples were cross-sectioned, polished and etched to check the bead profile and remelting area.

In PTA-based WAAM, the plasma arc is constricted by a water-cooled copper nozzle, which means the nozzle size affects the arc pressure and consequently keyhole formation. Therefore, in this study two different sized nozzles with diameters of 3.0 and 3.9 mm were used to investigate the effect of nozzle size on keyhole behaviour. For each size of nozzle, different levels of current were applied to study the effect of current on keyhole behaviour.

Two wires with diameters of 1.2 and 2.4 mm were used to study the effect of wire feeding position on the deposition process. Fig. 2 schematically shows the definition of the wire feeding position, where the distance between the wire and the substrate along the centreline of the torch is defined as h. For each size of wire, h was increased from 0 to 3.0 mm with an increment of 0.5 mm. The metal transfer behaviour was monitored using the process camera, and the bead dimensions were measured using a digital vernier caliper.

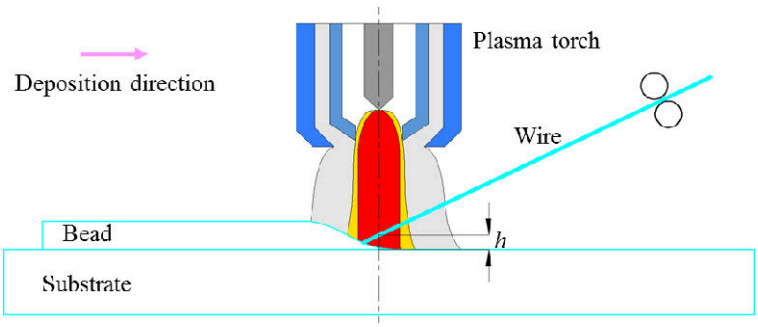

Fig. 2. Wire feeding position in PTA-based deposition process (side view).

3. Results and discussion

3.1 Limitation of deposition rate

Fig. 3 shows the melt pools for two different WFSs for a 1.6 mm wire at a current of 300 A. Up to a WFS of 5.4 m/min, the wire was completely melted, and the deposition process was stable (Fig. 3a). However, when the WFS was increased to 6.0 m/min the wire could not be melted completely and some violent disturbances occurred in melt pool, as exhibited in Fig. 3b. This is because when the WFS is too high, the volume of feedstock is too high for a given energy input to fully melt the wire, and this causes stabbing of the wire tip which disturbs the melt pool.

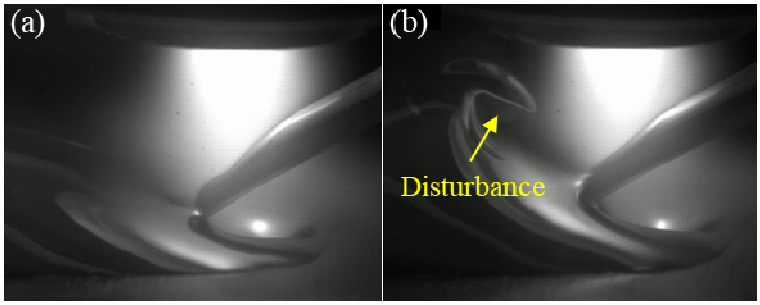

Fig. 3. Comparison between (a) stable deposition process at a WFS of 5.4 m/min, and (b) unstable deposition process at a WFS of 6.0 m/min.

The same experiment was repeated for all the remaining wire diameters. The maximum WFS for different sized wires under different currents is shown in Fig. 4. It can be seen that for each size of wire the maximum WFS increases with current. This is attributed to the increasing heat input as the current increases.

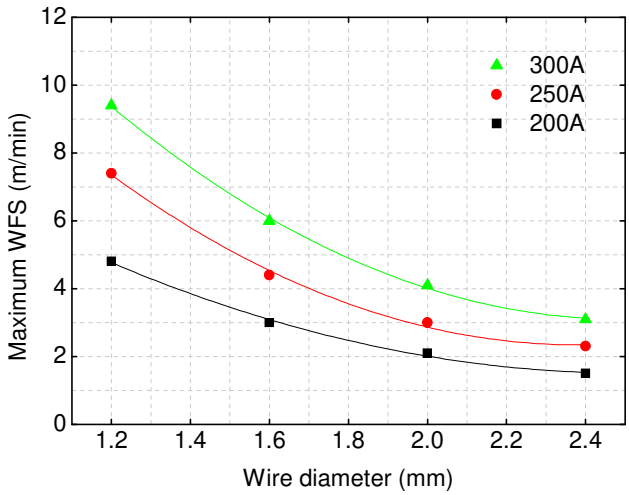

Fig. 4. Effect of wire size and current on maximum WFS.

From Fig. 4, one also can see that at a same current, the maximum WFS decreases with the increasing wire thickness. However the deposition rate, R, is expressed by:

$$R = \frac{\pi d^2 v \rho}{4} \tag{1}$$

where d is the wire diameter, v is WFS and ρ is the wire density. Therefore, with equation (1) and the data from Fig. 4, the deposition rate as a function of wire diameter was achieved, as shown in Fig. 5. It can be seen that for a particular current, the deposition rate increases linearly with wire size. This means that for the same energy input, a higher deposition rate can be achieved by using a thicker wire. This is because thick wire has larger width and consequently larger projected area under the arc, which enables it to capture more energy from the arc compared to thin wire.

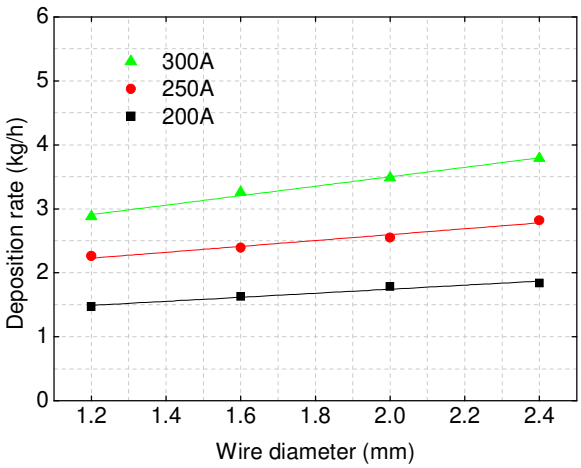

Fig. 5. Effect of wire size and current on the limitation of deposition rate.

The effect of wire diameter has been schematically shown in Fig. 6 with the projected areas of both wires under the plasma arc. It is assumed that the distribution of energy intensity of plasma arc is uniform, and the wire is only melted by arc. It can be seen that the projected area of 2.4 mm wire (area B) is twice as that of 1.2 mm wire (area A). Therefore, in a unit time 2.4 mm wire absorbs twice the energy as 1.2 mm wire regardless of their WFSs. This indicates that twice the volume of 2.4 mm wire can be melted as that of 1.2 mm wire per unit time. If the WFSs of the two wires can be adjusted to a certain level where the volume of the feeding material of 2.4 mm wire is twice as that of 1.2 mm wire per unit time, then both wires can be fully melted and consequently the deposition rate achieved with 2.4 mm is twice as that of 1.2 mm wire.

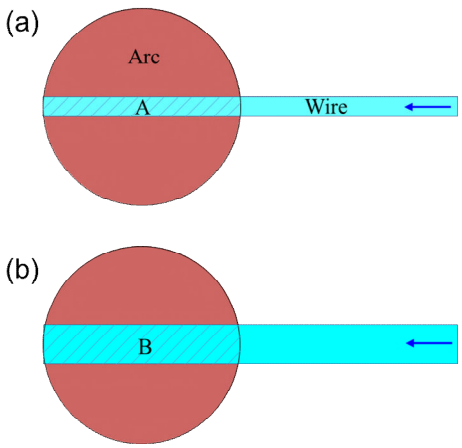

Fig. 6. The diagram (top view) shows the projected areas under plasma arc of (a) 1.2 mm and (b) 2.4 mm wires.

Also, a finite element (FE) modelling was conducted to support this explanation by using 1.2 and 2.4 mm wires. In the modelling work, a power of 2000 W was applied on both wires. To make both wires fully melted, the maximum WFSs obtained for 1.2 and 2.4 mm wires were 3.00 and 1.38 m/min respectively. The

temperature distributions of the two wires can be seen in Fig. 7. According to equation (1), the deposition rate of the 2.4 mm wire is around 1.84 times as that of 1.2 mm wire in this modelling work, which is close to the theoretical analysis. The difference is mainly because that the heat source applied in the modelling work is a Gaussian distribution instead of a uniform distribution.

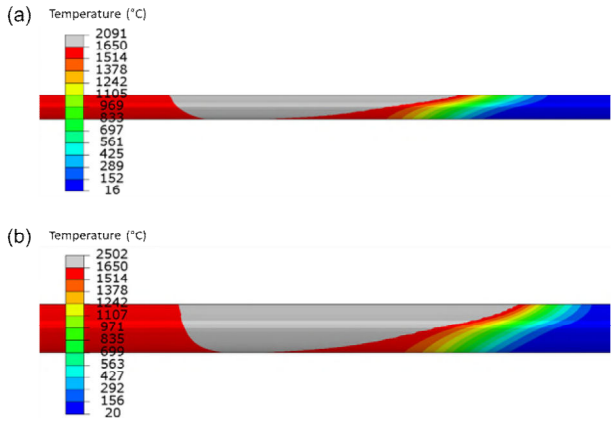

Fig. 7. The temperature contours of (a) 1.2 mm wire, and (b) 2.4 mm wire in the FE modelling.

In reality, the thick wire is not as efficient as both theoretical analysis and FE modelling (e.g., deposition rates of 1.84 and 1.47 kg/h for 2.4 and 1.2 mm wires respectively at 200 A, see Fig. 5). This is because that in theoretical analysis and FE modelling, the wires are only melted by arc. In practice, at high WFS the arc does not melt the feedstock completely, hence both 1.2 and 2.4 mm wires reach the melt pool, which provided extra energy to fully melt the wires (take Fig. 3 as an example). However, because the 2.4 mm wire shaded more energy from the arc so that the energy in the melt pool is lower. Therefore, the energy absorbed from the melt pool by the 2.4 mm wire cannot be as much as that of the 1.2 mm wire, resulting in a bit higher deposition rate of the 2.4 mm wire.

Fuerschbach and Knorovsky (1991) measured the melting efficiency in PTA and GTA welding processes in an edge weld configuration, and DuPont and Marder (1995) also measured the melting efficiency in GMA welding process. Both of them stated that a significant proportion of the total arc energy absorbed by the workpiece is dissipated for conduction losses, and only a small proportion is utilised for melting. Therefore, due to the less thermal loss of the wire compared to the workpiece, the melting efficiency is higher when using a thicker wire.

3.2 The effect of wire size on bead shape

In WAAM a single bead is the smallest and fundamental unit of a built part, hence the bead shape will determine the final surface waviness and consequently the deposition efficiency of the component. Fig. 8

shows a schematic representation of different regions in a generic part cross-section (Fig. 8a) and the surface waviness of two single pass walls with different bead shapes (Fig. 8b and 8c). Note that the volume of each single bead is the same for the two walls in Fig. 8b and 8c. As reported by Martina et al. (2012), the deposition efficiency, ε, is calculated as.

$$\varepsilon = \frac{A}{A + B + C + D} \tag{2}$$

where area A corresponds to the cross-section that can be used in the final part, whilst areas B, C and D correspond to the cross-sections that need to be machined off. It can be seen that a low aspect ratio (i.e., the ratio of bead width to bead height) of the bead will lead to a high surface waviness and low deposition efficiency (Fig. 8b), while a high aspect ratio of the bead with low and wide layer will ensure the near net shape and high deposition efficiency (Fig. 8c). This means that for the same deposited material more material needs to be machined away in the first wall (Fig. 8b), hence the second approach is more cost effective and desirable (Fig. 8c). Therefore, for a given wire feeding rate, the higher the aspect ratio of the bead, the better the surface finish and higher deposition efficiency of the component.

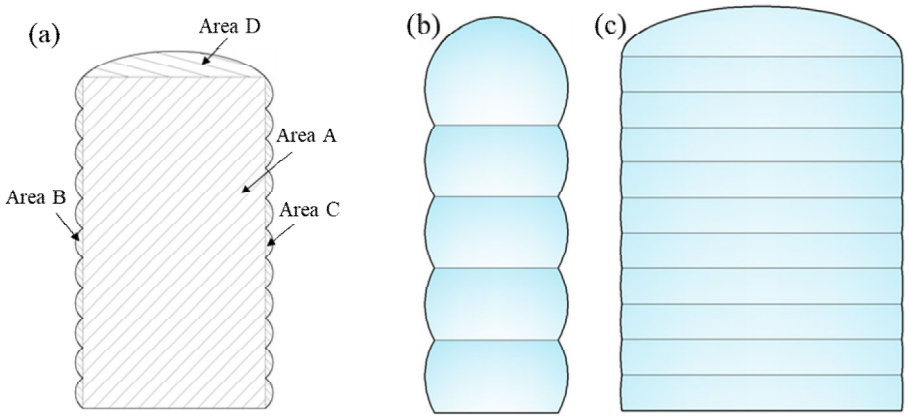

Fig. 8. (a) Schematic representation of deposition efficiency, (b) a high surface waviness but low deposition efficiency obtained by the bead with low aspect ratio, and (c) a low surface waviness but high deposition efficiency obtained by the bead with high aspect ratio.

Two wire diameters were used to deposit single layers with the same deposition rate and their dimensions were compared. Fig. 9 shows a comparison of the bead shape obtained by 1.2 and 2.4 mm wires at 250 A, and Fig. 10 shows corresponding cross-sections. In Fig. 9a, it can be seen that for both wires, as the deposition rate (controlled by WFS) increases the bead width increases gradually at first and then decreases slightly. The width of the melt pool without feeding the wire (8.07 mm) is also shown in Fig. 9a, which is

less than those with the wire feeding. The increasing bead width at relatively low deposition rates (from around 0.5 to 1.6 kg/h) is due to the increasing melting efficiency. This is because as the WFS increases, more energy is absorbed by wire and less energy is dissipated through workpiece. Therefore, this leads to an increasing melting efficiency and consequently wider beads. However, as the deposition rate further increases (from around 1.6 kg/h), the melt pool is being depleted of the heat and there is not enough heat to provide sufficient wetting with the substrate and this results in narrow and tall beads. An extra experiment was conducted to prove this as shown in Fig. 11, where the WFS was increased from 3 to 5 m/min in the first deposit and from 5 to 7 m/min in the second deposit. From the first case (Fig. 11a), it can be clearly seen that the bead width increases as the WFS increases. However, in the second case (Fig. 11b) the bead width decreases due to the wire dipping into the melt pool. As for the bead height (Fig. 9b), it increases constantly as the deposition rate increases due to the increase of the feeding material.

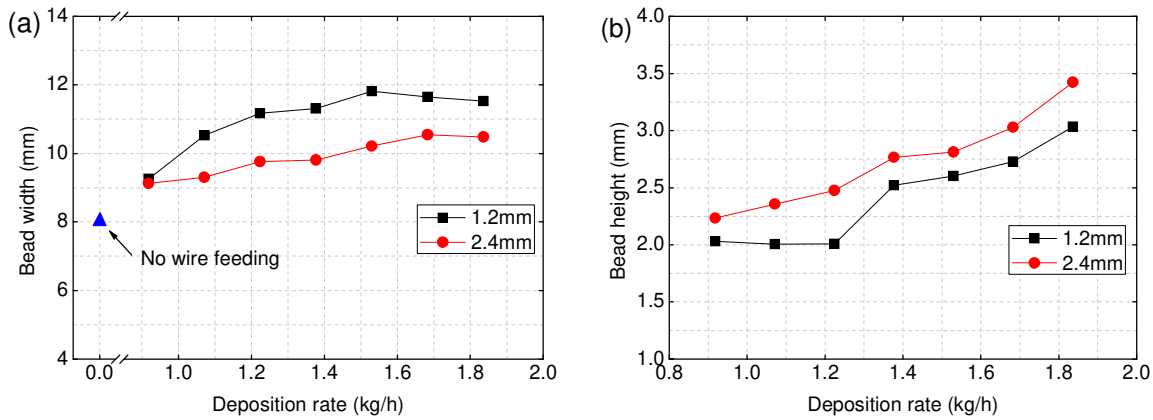

Fig. 9. Bead (a) width and (b) height as a function of deposition rate for 1.2 and 2.4 mm wires at the current of 250 A.

Moreover, by comparing the bead shapes obtained by the two different wires in Fig. 9, one can see that at the same deposition rate the bead obtained by 1.2 mm wire is wider and lower compared to that of 2.4 mm wire, meaning that the former has a higher aspect ratio. As discussed in Section 3.1, due to the larger projected area under the arc, more energy goes to the thicker wire directly and less energy goes to the workpiece, leading to a smaller remelting area in the workpiece. This is consistent with the results presented in Fig. 10, where at a same deposition rate the remelting area in the workpiece with 2.4 mm wire is smaller than that of 1.2 mm wire (note, the remelting area is hard to identify, but its size can be reflected by the heat-affected zone). Therefore, it can be concluded that at a same current and deposition rate, a higher aspect ratio

of the bead can be obtained with a thinner wire, which will lead to a better surface finish and higher deposition efficiency of the component.

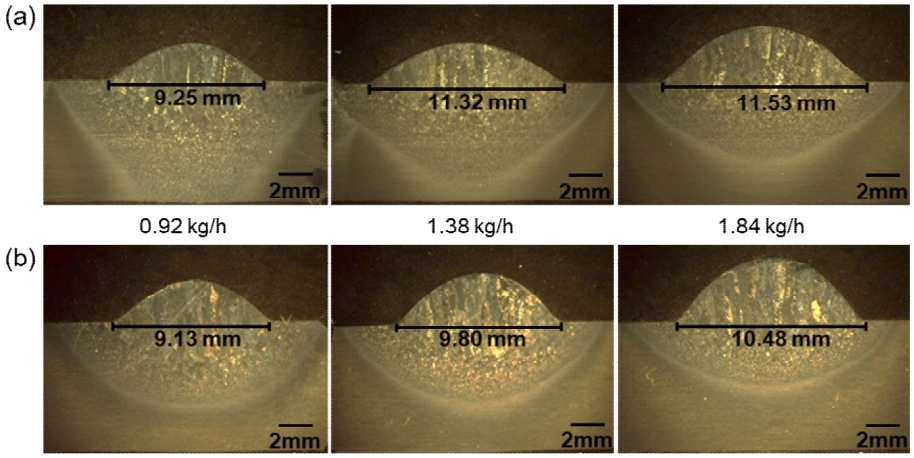

Fig. 10. Cross-section of the beads at different deposition rates obtained by (a) 1.2 mm wire, and (b) 2.4 mm wire at the current of 250 A.

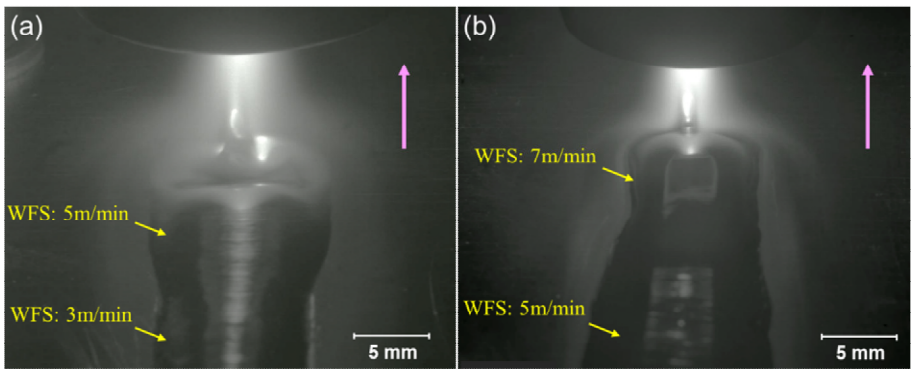

Fig. 11. Bead shape changes with the increasing WFS during deposition with 1.2 mm wire at 250 A: (a) bead width increases as WFS increases from 3 to 5 m/min, and (b) bead width decreases as WFS increases from 5 to 7 m/min. The pink arrow indicates the torch travel direction.

3.3 Keyhole behaviour

Jian and Wu (2015) reported that keyhole is formed under a combined effect of intensive energy and arc pressure, where the intensive energy melts the workpiece and the high pressure of the plasma jet produces a funnel-shaped cavity in the melt pool. Wu et al. (2019) developed an electrode-arc model and a 3D weld pool model to investigate the keyhole formation mechanism, and found that the arc pressure is the dominant driven force for the keyhole formation. Dai et al. (2002) investigated the effect of different process parameters on the arc pressure experimentally, including arc current, nozzle size, and plasma gas flowrate, and according to them the arc pressure is expressed by:

$$p = p_e + p_g = \frac{\mu_0 I^2}{4\pi^2}\left(\frac{1}{r_2^2} - \frac{1}{r_1^2}\right) + \frac{1}{2}\rho u_z^2 \quad (3)$$

where p_e is the pressure caused by electromagnetic force, p_g is the pressure caused by plasma gas flow, μ_0 is the magnetic permeability, I is the current, r_1 and r_2 are the radius of the arc at the workpiece and electrode, respectively, ρ is the plasma gas density, and u_z is the flow velocity of the plasma gas. It can be seen that the arc pressure consists of the pressure caused by electromagnetic force and the pressure caused by plasma gas force where the former depends on the current and the latter depends on the plasma gas flow velocity. Therefore, high current process and small nozzle diameter are likely to induce keyholes in the substrate or underlying layer which is undesirable in WAAM. This limits the maximum energy input that can be used for WAAM. Fig. 12 shows the keyhole appearances obtained with a stationary and a moving torch respectively without feeding the wire. In Fig. 12a, there is a large depression in the centre of the melt pool due to the high arc pressure, where the liquid metal has been pushed away from the centre. In Fig. 12b, the keyhole caused visible defects which was not subsumed by the liquid metal before solidification took place.

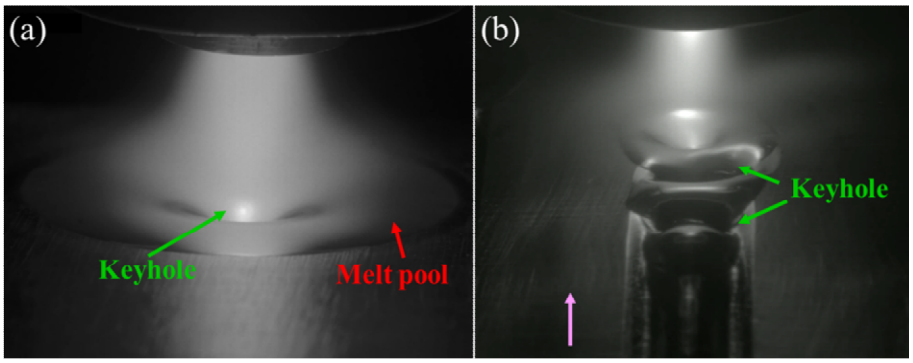

Fig. 12. Keyhole appearance with a (a) stationary and (b) moving plasma torch.

Fig. 13 shows the cross-sections of the samples under different currents and nozzle sizes with a stationary plasma torch. Note that no wire was fed in this case. From Fig. 13a, it can be seen that there is a funnel-shaped cavity in each sample where 3.0 mm nozzle was used, and the cavity becomes larger as the current increases. The formation of the cavity is due to incomplete closure of the keyhole caused by displacement of the liquid metal by arc pressure. Both energy input and arc pressure (p_e) increase as the current increases, which results in a greater keyhole size and consequently a larger cavity. However, there is no cavity formed at the current of 200 and 250 A with 3.9 mm nozzle, as shown in Fig. 13b. This shows that the keyhole susceptibility decreases with an increase in nozzle size. This is because when the area of the nozzle exit

increases, the flow velocity of the plasma gas decreases, which reduces the arc pressure (p_g) and leads to a lower likelihood of keyhole.

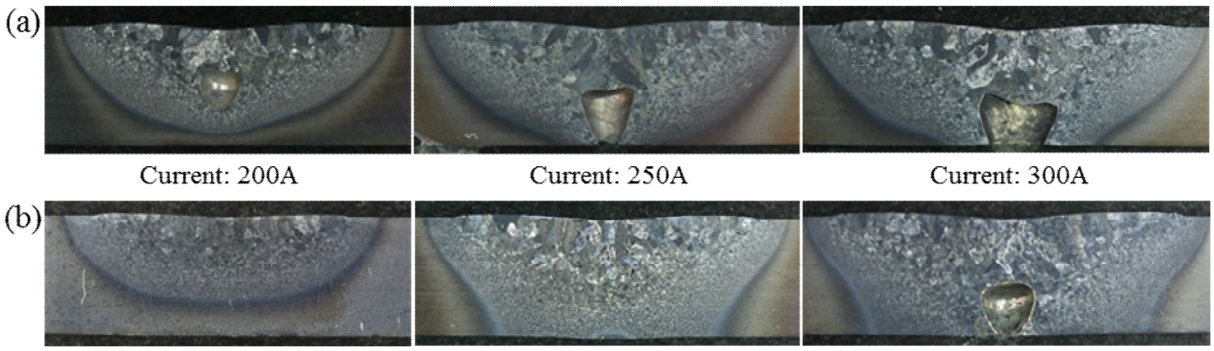

Fig. 13. The cross-section of the samples with different currents and nozzle diameters: (a) 3.0 mm nozzle, and (b) 3.9 mm nozzle. The plasma torch was stationary.

Some experiments with a moving plasma torch were also conducted without feeding the wire, and the appearance of the samples is shown in Fig. 14. It can be seen from Fig. 14a that by using a 3.0 mm nozzle there is no obvious defect at a current of 200 A, but a defect caused by keyhole was generated at a current of 260 A. However, when using a 3.9 mm nozzle no defect was found at both 200 and 260 A, as shown in Fig. 14b. Generally, the nozzles used in traditional PTA welding and cutting processes are less than 3.0 and 1.5 mm, respectively. Therefore, the nozzles used in the above experiments are relatively large. A 3.9 mm nozzle was adopted in all experiments of this study to decrease the likelihood of keyhole formation.

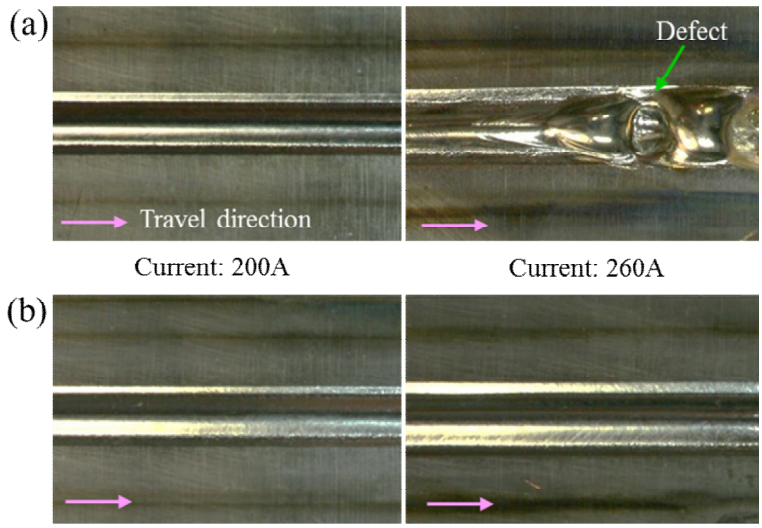

Fig. 14. The appearance of the samples obtained with different currents and nozzle diameters: (a) 3.0 mm nozzle, and (b) 3.9 mm nozzle. The torch travel speed was 9.0 mm/s in these cases.

In the previous experiments, there was no wire feeding. However, the keyhole behaviour may change with the presence of a filler wire as the wire can obscure the plasma arc and reduce its impact on the workpiece. Fig. 15 shows the deposition process using wires with diameters of 1.2, 1.6, 2.0 and 2.4 mm. Note that the deposition rate and current were constant in all cases. It can be seen that the keyhole is quite significant when using a 1.2 mm wire (Fig. 15a), but it becomes smaller with a 1.6 mm wire (Fig. 15b). For 2.0 and 2.4 mm wires, the keyhole formation was completely suppressed (Fig. 15c and d). This is attributed to the screening of plasma arc by the wire. With thin wires only a small portion of the arc energy interacts directly with the wire and most of it reaches the workpiece. However, as the wire diameter increases the ability of wire to obscure the arc increases and less energy is available to heat up the underlying workpiece, and a significant proportion of the electromagnetic force acts directly on the wire. This changes the energy balance between workpiece and wire while simultaneously suppressing the keyhole formation.

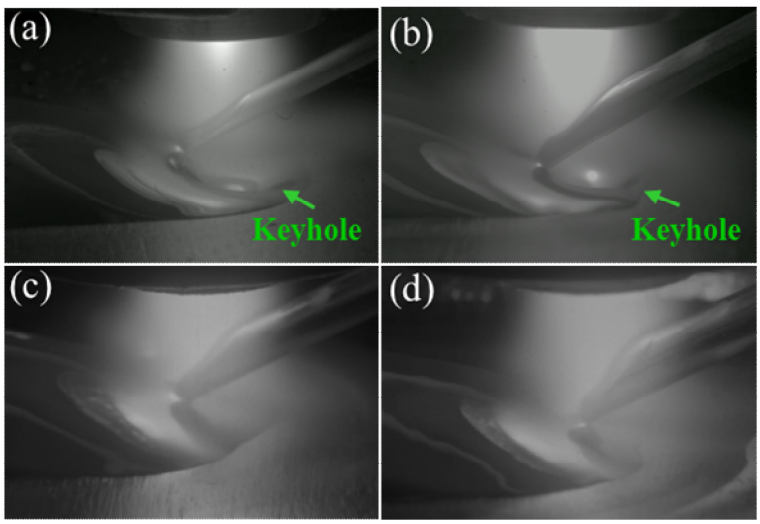

Fig. 15. Effect of wire size on keyhole formation at 300 A for the following wire diameters: (a) 1.2 mm, (b) 1.6 mm, (c) 2.0 mm, and (d) 2.4 mm.

3.4 Wire feeding position

In wire based AM processes, there are mainly three types of metal transfer modes which are surface tension transfer (also known as liquid bridge transfer), droplet surface tension transfer (also known as intermediate transfer), and free space droplet transfer (also named as droplet transfer). Ríos et al. (2019) stated that the stability of the process and the metal transfer mode are largely governed by the wire feeding position. Fig. 16 shows the deposition process and the bead width with different wire feeding positions at two different WFSs obtained with a 1.2 mm wire. At a low WFS of 3.2 m/min (Fig. 16a), the wire can be

melted sorely by the arc regardless of the wire feeding position. However, at a very low position (h=0 mm), the droplet touches the melt pool, which leads to a droplet surface tension transfer mode. When the wire feeding position is higher, the metal transfer turns into a free space droplet transfer mode. From Fig. 16c, it can be seen that the bead width does not change so much with the increase of wire feeding position. At a high WFS of 4.4 m/min (Fig. 16b), when the wire feeding position is low ($0 \leq h < 2.5$mm), the wire passes through the plasma arc and reaches the melt pool, leading to a surface tension transfer mode. As the wire feeding position increases from 2.5 to 3.0 mm, the metal transfer changes from a droplet surface tension to a free space droplet transfer mode.

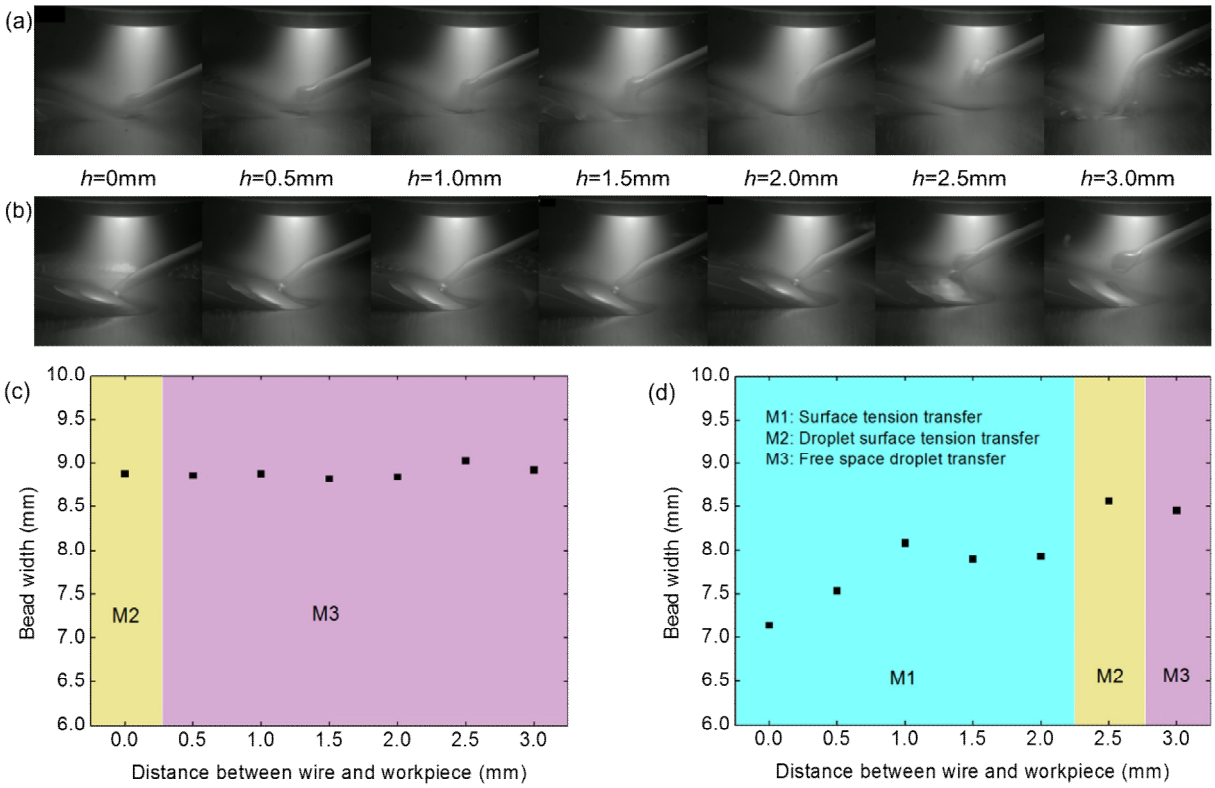

Fig. 16. The deposition process with different wire feeding positions at the WFS of (a) 3.2 m/min (deposition rate: 0.98 kg/h), and (b) 4.4 m/min (deposition rate: 1.35 kg/h) by using a 1.2 mm wire. Bead width and metal transfer mode as a function of h: (c) WFS=3.2 m/min, (d) WFS=4.4 m/min.

When the WFS is low, the wire is fully melted by the arc before it reaches the melt pool, which does not affect the metal transfer behaviour so much. However, when the WFS is high, the metal transfer mode is affected by the wire feeding position. This is mainly because there is a temperature gradient in the plasma arc where the temperature increases from the bottom to the top region as reported by Chu and Lian (2004). In the high WFS case, when the wire feeding position is low, the wire could not be fully melted only by the

arc, which means that additional energy needs to be taken from the melt pool. This depletion of energy from the melt pool by the wire results in a narrow bead shape. However, when the wire is positioned in the upper region of the plasma arc near the cathode where the plasma arc is more focused, the wire could be completely melted by the arc without interacting with the melt pool. This is the main reason that the bead width obtained with surface tension transfer mode is narrower than those of droplet surface tension and free space droplet transfer modes, as shown in Fig. 16d.

The same experiment was replicated for 2.4 mm wire with the same deposition rates as those of 1.2 mm wire, and the results are shown in Fig. 17. At both WFSs of 0.8 m/min (Fig. 17a) and 1.1 m/min (Fig. 17b), as the wire feeding position increases from 0 to 3 mm, the metal transfer changes from surface tension transfer mode to droplet surface tension transfer mode, and then to free space droplet transfer mode. Similarly to the previous case, the bead width in surface tension transfer mode is lower than in droplet surface tension and free space droplet transfer modes (Figs. 17c and 17d). This is attributed to depletion of heat from melt pool by the wire as discussed earlier.

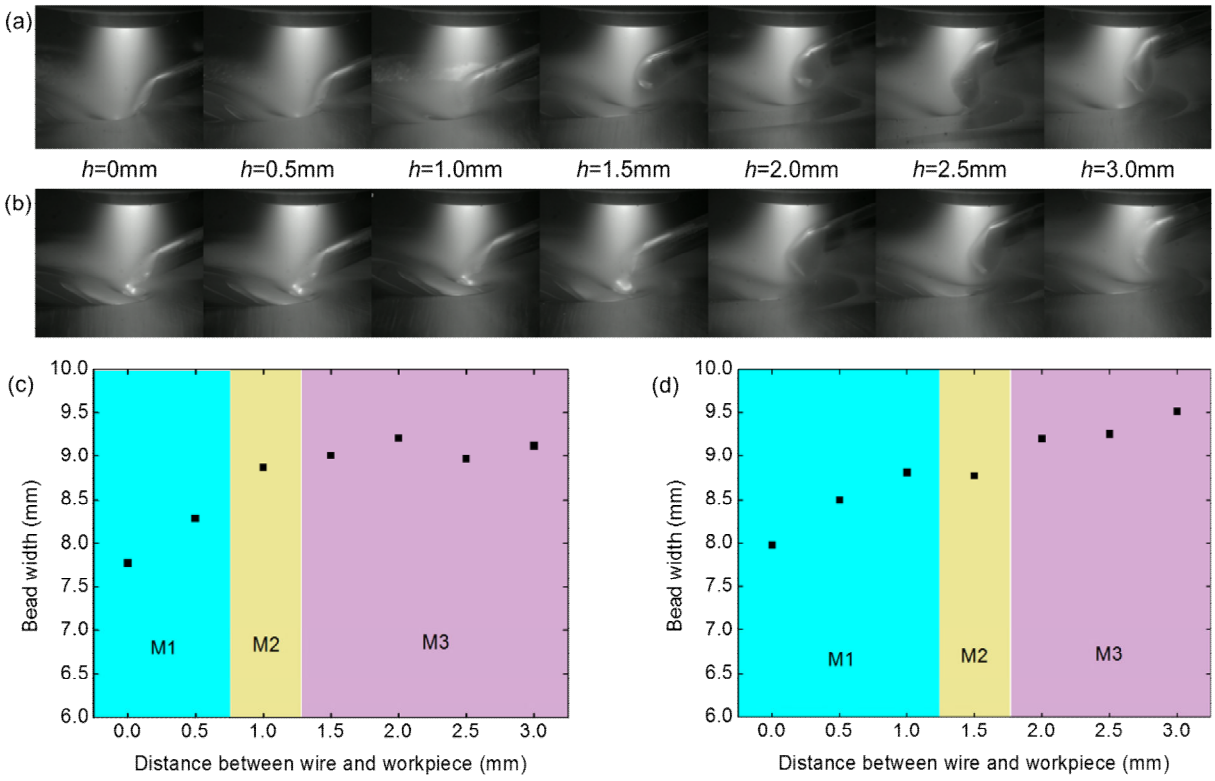

Fig. 17. The deposition process with different wire feeding positions at the WFS of (a) 0.8 m/min (deposition rate: 0.98 kg/h), and (b) 1.1 m/min (deposition rate: 1.35 kg/h) by using 2.4 mm wire. Bead width and metal transfer mode as a function of *h*: (c) WFS=0.8 m/min, (d) WFS=1.1 m/min.

By comparing the results obtained with 1.2 mm and 2.4 mm wires, it can be seen that at two different deposition rates of 0.98 and 1.35 kg/h, the droplet surface tension transfer mode occurred at the *h* of 0 and 2.5 mm respectively for 1.2 mm wire. However, this transfer mode occurred at two very close wire feeding positions (at the *h* of 1.0 and 1.5 mm, respectively) for 2.4 mm wire. This means the transition of the metal transfer mode depends on the wire diameter, and 1.2 mm wire is more sensitive to the wire feeding position than 2.4 mm wire as the deposition rate increases. This is mainly because that the thick wire interacts more with the arc than the thin wire due to the bigger projected area and longer interaction time (attributed to lower WFS for the same deposition rate), which means that the it interacts less with the melt pool. This also can be seen from Figs. 16b and 17b where the 1.2 mm wire reaches the middle part of the melt pool in surface tension transfer mode, while the 2.4 mm wire reaches the leading edge of the melt pool. The lower likelihood of interaction of thicker wire with the melt pool makes the process less sensitive to variation of transfer mode.

It can be seen that compared to surface tension transfer mode the beads obtained with droplet surface tension and free space droplet modes are wider. However, because of the erratic mode of the free space droplet transfer, spatter occurs occasionally in this case. Therefore, droplet surface tension transfer is recommended in WAAM process, which not only gives a wider bead but also gives a more stable process. In addition, Ríos et al. (2019) reported that this mode is easier to be detected compared to other transfer modes, and therefore it is more preferable in terms of process monitoring with closed loop feedback system when using robotic processes.

Based on the obtained results it can be seen that thicker wire is more efficient in terms of achieving high deposition rate (Fig. 5). For a fixed current a considerably higher build rate can be achieved with bigger diameter wire (e.g., 3.8 kg/h for 2.4 mm wire versus 2.9 kg/h for 1.2 mm wire for 300 A). Alternatively for a given build rate the current required is lower as the wire diameter increases. This means that with thicker wires we can achieve a higher deposition rate using the same energy input, or we can use a lower energy input to achieve the same deposition rate. Also, the thick wire can block more arc than the thin wire, which can mitigate the keyhole. In addition, as the deposition rate increases the metal transfer is not so sensitive to the wire feeding position for thick wire. This means that in order to keep the same metal transfer mode in a part building process, the wire feeding position for thick wire does not need to be adjusted oftentimes as the WFS changes. However, at a same current and deposition rate the bead shape obtained with the thinner wire has a higher aspect ratio, which is better for the surface finish of the component. In practice, thicker wires

are more challenging for the feeding system due to their stiffness. For example, the 2.4 mm diameter wire was very hard to manipulate, especially when building parts with complex shapes, which required continuous rotation of the wire position around the plasma torch. Therefore, there will be a trade-off between the hardware and the thickest wire that can be used, meaning that the hardware of the system needs to be improved in order to use thicker wires.

4. Conclusions

1. For all the four wire sizes investigated in this study, more material could be melted with increasing current due to a higher heat input. At the same current, the maximum deposition rate increases linearly with the wire size, which is caused by direct heating of the wire by the arc and lower amount of heat being transferred to the workpiece. A very high deposition rate of 3.8 kg/h could be achieved with a current of 300 A by using 2.4 mm wire.
2. For the same current and deposition rate, the bead obtained with 1.2 mm wire exhibited higher aspect ratio than that of 2.4 mm wire, therefore this wire allows achievement of lower surface waviness during part building. Besides, the 1.2 mm wire was much easier to manipulate than the 2.4 mm wire.
3. Both the heat input and electromagnetic force increase with increasing current of plasma arc, leading to the formation of keyhole. The keyhole formation can be mitigated by using larger diameter nozzles due to lower pressure of plasma gas. Keyhole can also be mitigated by using thicker wires due to the screening of the arc.
4. As the wire feeding position becomes higher from the substrate, the metal transfer changes from surface tension transfer mode to droplet surface tension transfer mode and then to a free space droplet transfer mode, which leads to an increasing bead width. The droplet surface tension transfer mode was found to give the most optimum bead shape and stable deposition with high enough tolerance. As the deposition rate increases, the metal transfer mode of thin wire is more sensitive to the wire feeding position than thick wire.

Acknowledgement

Chong Wang would like to express his gratitude to Cranfield University and China Scholarship Council (No. 201706450041) for funding his research studies. The authors would like to thank NEWAM (EP/R027218/1) and WAAMMat programmes for the financial support. The authors also would like to thank Flemming Nielsen, Nisar Shah, John Thrower, and Steve Pope for the technical support.

Reference

Caballero, A., Ding, J., Bandari, Y., Williams, S., 2019. Oxidation of Ti-6Al-4V during Wire and Arc Additive Manufacture. 3D Print. Addit. Manuf. 6, 91–98. https://doi.org/10.1089/3dp.2017.0144

Chu, S.C., Lian, S.S., 2004. Numerical analysis of temperature distribution of plasma arc with molten pool in plasma arc melting. Comput. Mater. Sci. 30, 441–447. https://doi.org/10.1016/j.commatsci.2004.03.014

Dai, D.S., Song, Y.L., Zhang, H., Zhu, Y.F., 2002. Study on arc force in plasma welding. Trans. China Weld. Inst. 23, 51–54. http://en.cnki.com.cn/Article_en/CJFDTotal-HJXB200202013.htm

DebRoy, T., Wei, H.L., Zuback, J.S., Mukherjee, T., Elmer, J.W., Milewski, J.O., Beese, A.M., Wilson-Heid, A., De, A., Zhang, W., 2018. Additive manufacturing of metallic components – Process, structure and properties. Prog. Mater. Sci. 92, 112–224. https://doi.org/10.1016/j.pmatsci.2017.10.001

Ding, J., Colegrove, P., Martina, F., Williams, S., Wiktorowicz, R., Palt, M.R., 2015. Development of a laminar flow local shielding device for wire + arc additive manufacture. J. Mater. Process. Technol. 226, 99–105. https://doi.org/10.1016/j.jmatprotec.2015.07.005

DuPont, J.N., Marder, A.R., 1995. Thermal efficiency of arc welding processes. Weld. J. (Miami, Fla) 74, 406-s. https://canteach.candu.org/Content%20Library/20053408.pdf

Frazier, W.E., 2014. Metal additive manufacturing: A review. J. Mater. Eng. Perform. 23, 1917–1928. https://doi.org/10.1007/s11665-014-0958-z

Jian, X., Wu, C.S., 2015. Numerical analysis of the coupled arc-weld pool-keyhole behaviors in stationary plasma arc welding. Int. J. Heat Mass Transf. 84, 839–847. https://doi.org/10.1016/j.ijheatmasstransfer.2015.01.069

Fuerschbach, P.W., Knorovsky, G.A., 1991. A study of melting efficiency in plasma - Desconhecido.pdf. Weld.

Res. Suppl. 287–297. https://app.aws.org/wj/supplement/WJ_1991_11_s287.pdf

Martina, F., Mehnen, J., Williams, S.W., Colegrove, P., Wang, F., 2012. Investigation of the benefits of plasma deposition for the additive layer manufacture of Ti-6Al-4V. J. Mater. Process. Technol. 212, 1377–1386. https://doi.org/10.1016/j.jmatprotec.2012.02.002

Pardal, G., Martina, F., Williams, S., 2019. Laser stabilization of GMAW additive manufacturing of Ti-6Al-4V components. J. Mater. Process. Technol. 272, 1–8. https://doi.org/10.1016/j.jmatprotec.2019.04.036

Ríos, S., Colegrove, P.A., Williams, S.W., 2019. Metal transfer modes in plasma Wire + Arc additive manufacture. J. Mater. Process. Technol. 264, 45–54. https://doi.org/10.1016/j.jmatprotec.2018.08.043

Shi, X., Ma, S., Liu, C., Chen, C., Wu, Q., Chen, X., Lu, J., 2016. Performance of high layer thickness in selective laser melting of Ti6Al4V. Materials (Basel). 9, 1–15. https://doi.org/10.3390/ma9120975

Wang, Y., Qi, B., Cong, B., Yang, M., Liu, F., 2017. Arc characteristics in double-pulsed VP-GTAW for aluminum alloy. J. Mater. Process. Technol. 249, 89–95. https://doi.org/10.1016/j.jmatprotec.2017.05.027

Williams, S.W., Martina, F., Addison, A.C., Ding, J., Pardal, G., Colegrove, P., 2016. Wire + Arc additive manufacturing. Mater. Sci. Technol. (United Kingdom) 32, 641–647. https://doi.org/10.1179/1743284715Y.0000000073

Wu, D., Van Nguyen, A., Tashiro, S., Hua, X., Tanaka, M., 2019. Elucidation of the weld pool convection and keyhole formation mechanism in the keyhole plasma arc welding. Int. J. Heat Mass Transf. 131, 920–931. https://doi.org/10.1016/j.ijheatmasstransfer.2018.11.108

2020-07-25

The effect of wire size on high deposition rate wire and plasma arc additive manufacture of Ti-6Al-4V

Wang, Chong

Elsevier

Wang C, Suder W, Ding J, Williams S. (2021) The effect of wire size on high deposition rate wire and plasma arc additive manufacture of Ti-6Al-4V. Journal of Materials Processing Technology, Volume 288, February 2021, Article number 116842

https://doi.org/10.1016/j.jmatprotec.2020.116842